Electronic structure of Ag-adsorbed nanowire-like stripes on Si(110)-(16×2) surfaces. II. A one-dimensional tight-binding model with Green's function approach

K. Bhattacharjee,[1] A. Roy,[1] K. Kundu,[1,2] and B. N. Dev[1,3,*]
[1]*Institute of Physics, Sachivalaya Marg, Bhubaneswar 751005, India*
[2]*Visva-Bharati, Santiniketan 731 235, West Bengal, India*
[3]*Department of Materials Science, Indian Association for the Cultivation of Science, 2A and 2B Raja S. C. Mullick Road, Jadavpur, Kolkata 700032, India*
(Received 19 December 2007; published 18 March 2008)

Si(110)-(16×2) surface has nanowire-like stripes, where the separation between stripes is ~5 nm. We initially ignore the interaction between these stripes and treat a stripe as a one-dimensional (1D) system. We have carried out a 1D tight-binding model calculation by considering various modified chains. In theoretical analysis of the model, real space renormalization technique and Green's function approach are adopted. The results obtained from the 1D model are consistent with the observed features in the local density of states. Scanning tunneling spectroscopy results obtained on the stripes of the Si(110)-(16×2) structures following a low-coverage Ag deposition show the following features: (i) band gap broadening, (ii) band gap variation, (iii) band offset, and (iv) appearance of new electronic states within the band gap. Our model qualitatively explains these features.

DOI: 10.1103/PhysRevB.77.115431 PACS number(s): 73.20.−r, 81.07.−b, 73.22.−f

I. INTRODUCTION

Si(110) surface with a particular surface reconstruction, namely, (16×2) reconstruction, shows a nanowire-like structure. The (16×2) reconstructed Si(110) surface consists of equally spaced and alternately raised and lowered stripes lying along the $[\bar{1}12]$ direction. The spacing between the adjacent raised stripes is about 5 nm and the width of a stripe is about 2 nm. Considering these features, the stripes on the Si(110)-(16×2) reconstructed surface may be assumed to represent a quasi-one-dimensional system. Adsorption of some elements on the stripes of the (16×2) reconstructed Si(110) surface and the evolution of the electronic structure would be interesting to investigate.

In order to investigate the electronic structure of the Si(110)-(16×2) surface with adsorbed atoms, we have carried out a one-dimensional (1D) tight-binding model calculation using Green's function formalism.[1] Since we are interested in explaining the band gap broadening, we primarily consider a periodic system.[2] However, we also consider the effect of impurities on the band dynamics in a limited way.

Structural details of Si(110) surface have been obtained from scanning tunneling microscopy (STM) measurements, which revealed that the reconstructed Si(110)-(16×2) surface consists of equally spaced and alternately raised and lowered "upstripes" and "downstripes" parallel to the $[\bar{1}12]$ direction which are separated by atomic steps of height $a_0/2\sqrt{2}$, where a_0 is the bulk lattice constant. The stripes consist of a zigzag pattern with a repetition distance of $\sqrt{6}a_0$.[3] The stripes are stacks of paired elements, the shape of which is interpreted differently by various authors as octets,[4] pentagons,[5] or centered stretched hexagons.[3] It has been observed that the (16×2) reconstruction occurs in two domains with the step boundaries along the $[\bar{1}12]$ or the $[1\bar{1}2]$ direction, where both domains form a periodic up and down sequence of terraces with a height difference of about one Si(110) bulk layer spacing (~0.19 nm).

Although some models of atomic arrangement on the 16×2 reconstructed surface have been proposed, there is no well-accepted model available.[6] To our knowledge, there are no theoretical studies of electronic structure of the (16×2) reconstructed surface.

In a companion paper, we present our investigation of the electronic structures of (i) a bare 16×2 surface and (ii) a Ag-adsorbed 16×2 surface by *in situ* scanning tunneling spectroscopy (STS) study. STS measurements were made by placing the STM tip over various points on 16×2 structures. Local density of states (LDOS) reveals an electronic band gap of around 1.1 eV, which corresponds to the bulk Si band gap. We have deposited an ultrathin Ag layer [$\frac{1}{8}$ ML (monolayer)] on these 16×2 structures in a molecular beam epitaxy system with the substrate at room temperature [1 ML $=0.96\times10^{15}$ atoms/cm^2, or the atomic density on an ideal Si(110) surface]. After Ag deposition, the surface was again characterized by *in situ* STM and STS measurements. STS spectra now taken at different points on the wirelike structures of Ag-adsorbed 16×2 surfaces show that the band gap of the surface has increased compared to the bulk Si band gap of 1.1 eV. We attempt to understand the experimental results, namely, (i) band gap broadening, (ii) band gap variation, (iii) band offset, and (iv) appearance of new electronic states within the band gap, by a one-dimensional tight-binding model calculation using Green's function formalism.

II. THEORETICAL MODEL

We construct a 1D model based on the Si(110)-(16×2) reconstructed structure as follows. The (16×2) structure with atomic arrangements is schematically shown in Fig. 1, which shows two upstripes, and a unit cell is marked.[3] As the separation between the stripes is ~5 nm, we assume this two be practically a 1D system and consider only one stripe, as shown in Fig. 2. We consider the atoms on the drawn line.

 ©2008 The American Physical Society

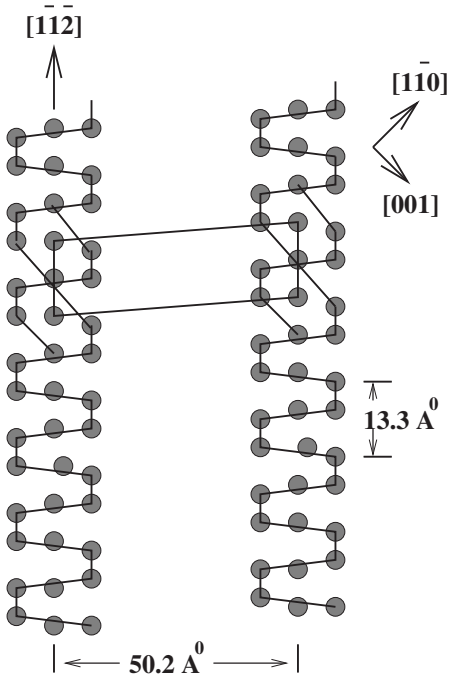

FIG. 1. Schematic representation of two upstripes or two downstripes of Si(110)-(16×2) structures. Surface unit cell is marked in the image (see Ref. 3).

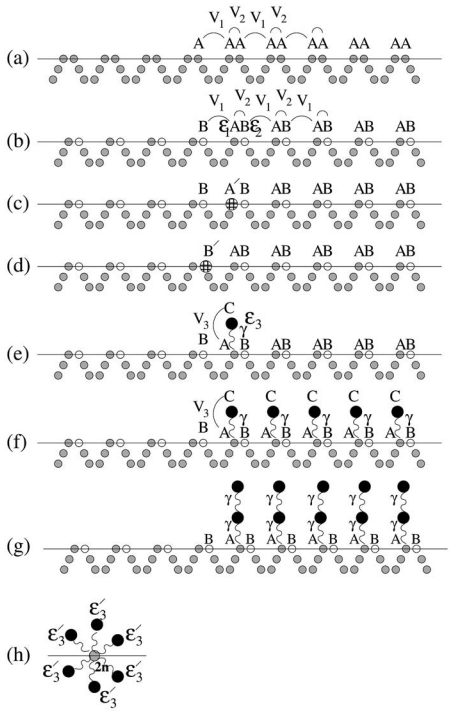

FIG. 2. A schematic model of Si(110)-(16×2) structures, which represents different cases before Ag deposition [Fig. 2(a)] and after Ag deposition [Figs. 2(b)–2(h)].

The system is now like each atom having a long bond on one side and a short bond on the other side. Effectively, this gives rise to two interaction parameters V_1 and V_2. When the effects of other atoms below the line are taken into account, one would still expect to have two different interaction parameters instead of identical ones. In this context, we note that STS spectra yield at least two main bands. This in turn implies that the system must have two different atoms per cell. Since the pure system is made up of Si only, the only way to realize effectively two atoms per cell is to have Si-Si bonds of two types, long and short. This is nearly represented by the structure shown in Fig. 2(a).

In order to understand the band gap broadening and other observed phenomena after Ag deposition, we have performed a 1D tight-binding model (TBM)[7] calculation to verify the local density of states and the associated increase in the band gap by using Green's function formalism.[1] Considering different cases of the quasi-1D model, we discuss below as to how this theoretical model can explain our experimental data. A schematic diagram of the cases discussed is shown in Fig. 2.

A. Description of the model

The atomic arrangements on the (16×2) reconstructed Si surface is schematically shown in Fig. 1. Based on this structure, we make the one-dimensional model, as shown in Fig. 2(a). The 1D structure is represented by the atoms on the line. We notice that the atoms, A, have two different A-A distances. They would have two interaction parameters V_1 (across the larger A-A distance) and V_2 (across the shorter A-A distance) and each A atom would have a site energy ε_1.[8]

We will describe the most general model and then discuss the specific cases represented by the diagrams in Figs. 2(a)–2(i).

If one A atom in a pair is replaced by a B atom [Fig. 2(b)], again we would have two different interaction parameters across the long and short bonds. These values would be different from those in Fig. 2(a). As these are only parameters, we still call them V_1 and V_2. The site energy for B atoms is ε_2. The motivation for considering the Ag-deposited Si surface as a one-dimensional AB system is as follows. The band gap in the system can arise from two situations: one due to the difference in tunneling and the other due to the difference in the site energies. Since Ag is deposited on the Si surface, this atom can go to one of the Si sites or Ag can interact with Si. In either case, we have to introduce different site energies. This will yield a bipartite or AB-type lattice.

In the ordered AB system, if an A atom is replaced by an impurity atom A' or a B atom is replaced by an impurity atom B', these cases are depicted in Figs. 2(c) and 2(d). Figure 2(e) depicts a situation where an A atom has a dangling bond, whatever its origin is, or an adsorbed atom represented by C and an interaction parameter $V_{3(2n)}$, where $2n$ is the site index. The most general case deals with the situation depicted in Fig. 2(f), where each A atom has a dangling bond or attached atom C. Amplitude equations of the electron then in the present TBM are given by

$$i\hbar \frac{dC_{2n}}{dt} = \varepsilon_1 C_{2n} + V_2 C_{2n+1} + V_1 C_{2n-1} + V_{3(2n)} X_{2n}, \quad (1)$$

$$i\hbar \frac{dC_{2n+1}}{dt} = \varepsilon_2 C_{2n+1} + V_1 C_{2n+2} + V_2 C_{2n}, \quad (2)$$

$$i\hbar\frac{dX_{2n}}{dt} = V_{3(2n)}C_{2n} + \varepsilon_{3(2n)}X_{2n}. \tag{3}$$

In this set of equations, A atoms are in the even sites, while B atoms are put in the odd sites. X denotes the amplitude of the electron at atom C. The formal derivation of these equations along with the corresponding tight-binding Hamiltonian is discussed in a more general way in Appendix A.

We now make the following transformations:

$$C_n \to C_n e^{-i\varepsilon_1 t/\hbar}, \tag{4}$$

$$X_{2n} \to X_{2n} e^{-i\varepsilon_1 t/\hbar}. \tag{5}$$

Furthermore, we take

$$\varepsilon_\circ = \varepsilon_F = \frac{\varepsilon_1 + \varepsilon_2}{2}, \quad \varepsilon = \frac{\varepsilon_1 - \varepsilon_2}{2}, \quad \varepsilon_1 = \overset{\circ}{\varepsilon}_F, \quad \varepsilon_F = \overset{\circ}{\varepsilon}_F - \varepsilon, \tag{6}$$

$$V = \frac{|V_1| + |V_2|}{2}, \quad \alpha = \frac{V_1}{V}, \quad \beta = \frac{V_2}{V},$$

$$\gamma_{2n} = \frac{V_{3(2n)}}{V}, \quad \alpha - \beta = \frac{2(V_1 - V_2)}{(|V_1| + |V_2|)}. \tag{7}$$

If $\alpha+\beta=2$, then both V_1, $V_2>0$. On the other hand, if $V_1>0$, $V_2<0$, then $\beta\to-\beta$ in the previous relation. Similarly, if $V_1<0$, $V_2>0$, we get $\alpha-\beta=-2$.

With the scaling,

$$\varepsilon \to \frac{\varepsilon}{V} \quad \text{and} \quad \tau = \frac{Vt}{\hbar} \tag{8}$$

along with performing a trite algebra, we finally get

$$i\frac{dC_{2n}}{d\tau} = \beta C_{2n+1} + \alpha C_{2n-1} + \gamma_{2n}X_{2n}, \tag{9}$$

$$i\frac{dC_{2n+1}}{d\tau} = -2\varepsilon C_{2n+1} + \alpha C_{2n+2} + \beta C_{2n}, \tag{10}$$

$$i\frac{dX_{2n}}{d\tau} = \gamma_{2n}C_{2n} + (\varepsilon_{3(2n)} - \varepsilon_1)X_{2n}, \quad n \in Z. \tag{11}$$

Here, one should note that all variables and parameters in Eqs. (9)–(11) are appropriately scaled. We now perform Laplace transformations with respect to a variable $E \in \mathbb{C}$, called energy henceforth, on this set of equations of motion and renormalize[9] the lattice, $2n\to n$ (see Fig. 3). At the end of these operations, we get the corresponding set of equations for the lattice Green's function,

$$[E - \Sigma_n(E)]G_{0,(nm)}(E) = \delta_{nm} + \tilde{V}(E)[G_{0,(n+1,m)}(E) + G_{0,(n-1,m)}(E)],$$

$$n,m \in Z \equiv (\text{integer set}), \tag{12}$$

where

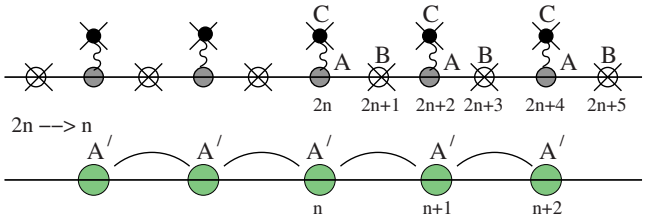

FIG. 3. (Color online) Schematic model which shows as how the renormalization is done for theoretical calculation. In the figure, "×" means decimation.

$$\Sigma_n(E) = \frac{\alpha^2 + \beta^2}{E + 2\varepsilon} + \frac{\gamma_n^2}{E + \varepsilon_1 - \varepsilon_{3(n)}}, \quad \tilde{V}(E) = \frac{\alpha\beta}{E + 2\varepsilon}. \tag{13}$$

In the case of $\varepsilon_{3(n)}=\varepsilon_3$ and $\gamma_{3(n)}=\gamma_3$ (totally perfect system), we can calculate the Green's function analytically. In this limit, after performing lattice Fourier transform on the appropriate variation of Eq. (12), we get

$$\sum_n e^{ikn}G_{0(nm)}(E) = \frac{e^{ikm}}{E - \Sigma(E) - 2\tilde{V}(E)\cos k}. \tag{14}$$

Putting $z=e^{ik}$, we get Green's function as

$$G_{0(nm)} = -\frac{1}{2i\pi\tilde{V}(E)}\oint_{c=1}\frac{z^{|m-n|}dz}{(z - z_+)(z - z_-)}. \tag{15}$$

Note that $c=1$ implies that the contour is a circle of unit radius around the origin in the complex z plane, $z \in \mathbb{C}$. $z_\pm$ are determined from

$$z^2 - \frac{E - \Sigma(E)}{\tilde{V}}z + 1 = 0. \tag{16}$$

Now, the contour integration [Eq. (15)] yields

$$G_{0(00)}(E) = \pm\frac{1}{\sqrt{[E - \Sigma(E) - 2\tilde{V}(E)][E - \Sigma(E) + 2\tilde{V}(E)]}}. \tag{17}$$

We consider next the following different cases to explain our results.

B. No dangling bond in the system

Let us consider the case where there is no dangling bond in the system [see Fig. 2(b)]. In this case, $\gamma=0$. Let us also consider that $\alpha\beta>0$. With these conditions, we get from the quadratic equation in E,

$$E - \Sigma(E) \pm 2\tilde{V}(E) = 0, \tag{18}$$

the results,

$$E_\pm = -\varepsilon \pm \sqrt{\varepsilon^2 + (\alpha \pm \beta)^2}, \tag{19}$$

where $E_\pm$ are the two roots of Eq. (18). Since $|\alpha+\beta|=2$, we get

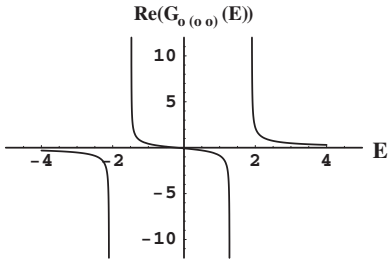

FIG. 4. Plot of the real part of Green's function calculated from theoretical model schematically shown in Fig. 2(b).

$$E_1 = -\varepsilon - \sqrt{\varepsilon^2 + 4}, \tag{20}$$

$$E_2 = -\varepsilon - \sqrt{\varepsilon^2 + (\alpha - \beta)^2}, \tag{21}$$

$$E_3 = -\varepsilon + \sqrt{\varepsilon^2 + (\alpha - \beta)^2}, \tag{22}$$

$$E_4 = -\varepsilon + \sqrt{\varepsilon^2 + 4}. \tag{23}$$

It should be noted here that these are the four real branch points of $G_{0(00)}$. Furthermore, $G_{0(00)}$ is real in the ranges $E_2 < E < E_3$, $E < E_1$, and $E > E_4$, otherwise stated $E \in \mathbb{R}$. Green's functions are in general complex functions of $E \in \mathbb{R} \subset \mathbb{C}$.

For $E_2 < E < E_3$, it can be shown that

$$G_{0(00)}(E) = -\frac{E + 2\varepsilon}{\sqrt{(E - E_1)(E - E_2)(E - E_3)(E - E_4)}}, \tag{24}$$

and for $E < E_1$ and $E > E_4$,

$$G_{0(00)}(E) = \frac{E + 2\varepsilon}{\sqrt{(E - E_1)(E - E_2)(E - E_3)(E - E_4)}}. \tag{25}$$

Plots of Eqs. (24) and (25) are shown in Fig. 4.

Now, the density of states $[\rho(E)]$ is obtained from the imaginary part of $G_{0(00)}(E)$ with $E \in \mathbb{C} \rightarrow E \in \mathbb{R}$. For the lower band ($E_1 < E < E_2$, $E \in \mathbb{R}$), $\rho(E)$ is

$$\rho_L(E) = \frac{1}{\pi} \frac{|E + 2\varepsilon|}{\sqrt{(E - E_1)(E_2 - E)(E_3 - E)(E_4 - E)}}. \tag{26}$$

For the upper band ($E_3 < E < E_4$, $E \in \mathbb{R}$), $\rho(E)$ is

$$\rho_u(E) = \frac{1}{\pi} \frac{|E + 2\varepsilon|}{\sqrt{(E - E_1)(E - E_2)(E - E_3)(E_4 - E)}}. \tag{27}$$

The band gap is

$$\Delta = E_3 - E_2 = \sqrt{\varepsilon^2 + (\alpha - \beta)^2}, \tag{28}$$

when $\varepsilon = 0$, i.e., $\varepsilon_1 = \varepsilon_2$,

$$\Delta = |\alpha - \beta| < \sqrt{\varepsilon^2 + (\alpha - \beta)^2}. \tag{29}$$

So, if we start with a system having all site energies equal to ε_1 and with no dangling bond, the band gap $\Delta = |\alpha - \beta|$. We note in this case again that the absolute band gap is given by $|V_1 - V_2|$ and the width of each band is the smaller of $|V_1|$ and $|V_2|$, ($|V_1| \wedge |V_2|$). The density of state plot from Eqs. (26) and (27) is shown in Fig. 5(i). The band gap Δ obtained from Eq. (29) is marked in Fig. 5 (i). From our STS data on the reconstructed Si surface considering the band gap and bandwidth, we find that for the short bond, the tunneling constant $V_2 \sim 1.6$ eV and the tunneling constant through the long bond, V_1, is ~ 0.5 eV. The band gap will increase further if along with the difference in tunneling there is also a difference in consecutive site energies. We note that the extra site energy $\varepsilon = (\varepsilon_2 - \varepsilon_1)/2$ can be calculated from the shift in the Fermi energy. Experimental value of this quantity is a fraction of an eV. The variability of the Fermi level is an indication of either variable Si-Ag interaction or replacement of a Si atom by a Ag atom. This in turn implies that the system may have some disorder (see the companion paper). However, periodicity with two atoms per unit cell is intact. For $\varepsilon_1 \neq \varepsilon_2$, i.e., $\varepsilon \neq 0$, the density of states is shown in Fig. 5(ii). The band gap, given by Eq. (28), is now larger compared to the case of $\varepsilon = 0$ [Fig. 5(i)]. A band offset is also seen in Fig. 5(ii). A case of further increase of band gap and larger band offset is shown in Fig. 5(iii). This case will be discussed later in Sec. II E. The model represented by Fig. 2(a), where all atoms are a same (A), say, Si as on the Si(110)-(16×2) reconstructed surface, provides a band gap [Eq. (29)]. When another kind of atom (B) is introduced [Fig. 2(b)], for example, Ag or some kind of Si-Ag complex, one obtains a band gap broadening [Eq. (28)] as well as a Fermi level shift [Eq. (6)]. This explains two aspects of the experimental observations.

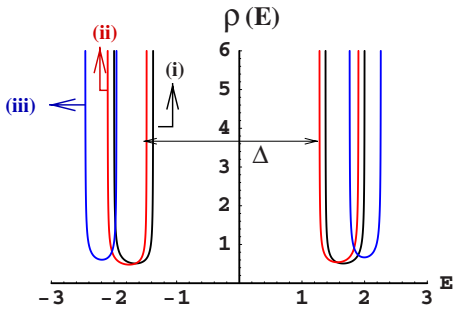

FIG. 5. (Color online) Plots of density of states which were obtained from theoretical model calculation. Here, all the expressions for density of states were calculated from a quasi-one-dimensional model. (i) represents the density of states of a pure $AAAA\cdots$ system, where no dangling atom interaction or the interaction coming from any other kind of impurity in the system have been considered. (ii) represents the density of states of a $ABAB\cdots$ model system. In this case also, we did not consider any interaction coming from dangling atom or any other kind of impurity. Here, every odd site atom A has been replaced by an atom B. The band gap has increased here by 0.0073 compared to the previous case (i). (iii) Density of states which have been calculated considering that each even site atom A interacts with a dangling atom C [see Fig. 6(f)]. We can see from the graph that the band gap has further increased due to the dangling atom interaction.

C. Problem of on site impurities

Here, we investigate the effect of a single diagonal impurity on the spectra. We note that the modified system we are

considering here has the morphology shown in Figs. 2(c) and 2(d).

We assume that there is a diagonal defect in the system. Otherwise, the system is perfect. It can happen in two different ways.

(i) The site energy of one of the even sites or A sites changes from 0 to ε' [see Fig. 2(c)].

(ii) The site energy of one of the odd sites or B sites changes from -2ε to $-2(\varepsilon+\varepsilon'')$ [see Fig. 2(d)].

In the following calculation, we keep both possibilities before embarking on one of the possibilities, but $\gamma=0$.

Now, applying condition (8) (making all quantities dimensionless), the equations of motion are given by

$$i\frac{dC_{2n}}{d\tau} = \beta C_{2n+1} + \alpha C_{2n-1}, \quad n \neq 0, \tag{30}$$

$$i\frac{dC_0}{d\tau} = \beta C_1 + \alpha C_{-1} + \varepsilon' C_0, \tag{31}$$

$$i\frac{dC_{2n+1}}{d\tau} = -2\varepsilon C_{2n+1} + \alpha C_{2n+2} + \beta C_{2n},$$

$$n = 0, \pm 1, \pm 2, \ldots, \tag{32}$$

$$i\frac{dC_1}{d\tau} = -2(\varepsilon+\varepsilon'')C_1 + \alpha C_2 + \beta C_0. \tag{33}$$

One should note that the system here contains two diagonal impurities. Performing Laplace transformation to these equations of motion and renormalizing the lattice in a similar fashion as in the previous case (decimating odd sites by letting $2n \to n$, see Fig. 3), we get the set of equations for the Green's function G_{nm} as

$$[E-\Sigma(E)]G_{nm} - \tilde{V}(E)[G_{n+1,m}(E) + G_{n-1,m}(E)] = \delta_{nm}, \tag{34}$$

$$n \neq 0,1,$$

$$[E-\Sigma_1(E)]G_{1m} - \tilde{V}(E)G_{2,m}(E) - \tilde{V}_{1,0}(E)G_{0,m}(E) = \delta_{1m}, \tag{35}$$

$$[E-\Sigma_0(E)]G_{0m} - \tilde{V}_{0,1}(E)G_{1,m}(E) - \tilde{V}(E)G_{-1,m}(E) = \delta_{0m}, \tag{36}$$

where

$$\Sigma(E) = \frac{\alpha^2+\beta^2}{E+2\varepsilon}, \tag{37}$$

$$\Sigma_0(E) = \varepsilon' + \frac{\alpha^2+\beta^2}{E+2\varepsilon} + \beta^2\left[\frac{1}{E+2(\varepsilon+\varepsilon'')} - \frac{1}{E+2\varepsilon}\right], \tag{38}$$

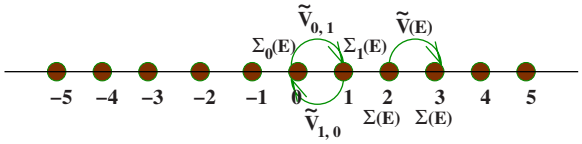

FIG. 6. (Color online) This figure represents the renormalized version of two diagonal impurities in the model. Here, $\Sigma(E)$ represents renormalized site energy. $\tilde{V}_{nm}$ represents renormalized tunneling.

$$\Sigma_1(E) = \frac{\alpha^2+\beta^2}{E+2\varepsilon} + \beta^2\left[\frac{1}{E+2(\varepsilon+\varepsilon'')} - \frac{1}{E+2\varepsilon}\right], \tag{39}$$

$$\delta\Sigma_0(E) = \varepsilon' + \beta^2\left[\frac{1}{E+2(\varepsilon+\varepsilon'')} - \frac{1}{E+2\varepsilon}\right], \tag{40}$$

$$\delta\Sigma_1(E) = \delta\Sigma_0(E) - \varepsilon', \tag{41}$$

$$\Sigma_0(E) = \Sigma(E) + \delta\Sigma_0(E), \tag{42}$$

$$\Sigma_1(E) = \Sigma(E) + \delta\Sigma_1(E), \tag{43}$$

$$\tilde{V}(E) = \frac{\alpha\beta}{E+2\varepsilon}, \tag{44}$$

$$\tilde{V}_{0,1}(E) = \frac{\alpha\beta}{E+2(\varepsilon+\varepsilon'')} = V_{1,0}(E). \tag{45}$$

We see that the renormalized system in this case has two consecutive diagonal impurities, which are connected by an effective interaction term which is different from the rest. So, the effective system is a system of two diagonal impurities and one off-diagonal impurity (Fig. 6). Following the standard procedure given in Appendix B, we get

$$G_{nm} = G_{0,nm} + \sum_{R,k} G_{0,nl}H_{lk}G_{km}. \tag{46}$$

In the following calculation, we set $\varepsilon''=0$. We then get a perfect system with one diagonal impurity. In this case, we have the following expression for the zeroth site Green's function (G_{00}) of the effective system:[1]

$$G_{00}(E) = \frac{G_{0(00)}(E)}{[1-\varepsilon' G_{0(00)}(E)]}. \tag{47}$$

Hence, the system will have a localized state coming from the pole of $G_{00}(E)$. $G_{0(00)}(E)$ is the zeroth site Green's function for the perfect system given by Eq. (17). Furthermore, the system has two localized states due to two bands in the system. In the case of infinitely many bands, we shall get infinite many localized states (the Kronig–Penny model[10]). The equation to obtain the energy of the localized state is given by the following:

$$\frac{1}{\varepsilon'} = G_{0(00)}(E).$$

Since $|G_{0(0,0)}| \uparrow \infty$ at band edges in this case, we shall have two localized states irrespective of the value of ε'. We already have the expression for $G_{0(0,0)}(E)$. So, if $\varepsilon' > 0$, we shall get two localized states above the bands. On the other hand, if $\varepsilon' < 0$, we again have two localized states. However, in this case, they appear below the bands. However, in both cases, we have a localized state in the band gap. In the first case, it is closer to the lower band, while in the other case, it is closer to the upper band.

In other limit $\varepsilon' = 0$ but $\varepsilon'' \neq 0$, we can integrate the even sites and keep equations of odd sites. Following the same procedure, we shall get an equation analogous to Eq. (47).

We note that even if both ε' and ε'' are nonzero, we can still solve for localized states. Theoretically, there cannot be more than four localized states. However, the number of localized states cannot be less than 2. We see here that any diagonal impurity splits a state from the band. So, we can say that in the impure system, the bandwidth will decrease. This particular one impurity problem presented here is to show the effect of diagonal impurity on the bandwidth. Similar results will be obtained if we have only an off-diagonal impurity in the system. Localized states in the band gap will also appear in the system having both diagonal and off-diagonal impurities. This model calculation shows one possible route for the appearance of electronic states within the band gap, as observed in the STS results obtained from the Ag-deposited Si(110)-(16×2) reconstructed surface.

D. Single dangling atom impurity

Here, we consider only one dangling atom impurity in the system sitting on the zeroth site [see Fig. 2(e)]. The amplitude equations of motion are

$$i\frac{dC_{2n}}{d\tau} = \beta C_{2n+1} + \alpha C_{2n-1}, \quad n \neq 0, \tag{48}$$

$$i\frac{dC_0}{d\tau} = \beta C_1 + \alpha C_{-}1 + (\varepsilon_3 - \varepsilon_1)X_0, \tag{49}$$

$$i\frac{dC_{2n+1}}{d\tau} = -2\varepsilon C_{2n+1} + \alpha C_{2n+2} + \beta C_{2n},$$

$$n = 0, \pm 1, \pm 2, \ldots,$$

$$i\frac{dX_0}{d\tau} = \gamma C_0 + (\varepsilon_3 - \varepsilon_1)X_0. \tag{50}$$

The set of renormalized equation which determines the Green's function of the system under renormalization (obtained by decimating the odd sites and renumbering the sites by $2n \rightarrow n$, see Fig. 3) is as follows:

$$[E - \Sigma(E)]G_{nm} - \tilde{V}(E)[G_{n+1,m}(E) + G_{n-1,m}(E)] = \delta_{nm},$$

$$n \neq 0,$$

$$[E - \Sigma_0(E)]G_{0m} - \tilde{V}(E)[G_{1,m}(E) + G_{-1,m}(E)] = \delta_{0m},$$

where

$$\Sigma(E) = \frac{\alpha^2 + \beta^2}{E + 2\varepsilon}, \tag{51}$$

$$\Sigma_0(E) = \Sigma(E) + \frac{\gamma^2}{E - (\varepsilon_3 - \varepsilon_1)}, \quad \tilde{V}(E) = \frac{\alpha\beta}{E + 2\varepsilon}.$$

It is a single defect problem with the defect situated at the origin of the renormalized system. We note that $\varepsilon_1 = \varepsilon_F^{\circ}$ (by definition). Following the standard procedure for the single impurity problem, we get the expression for Green's function as

$$G_{00} = \frac{G_{0(00)}(E)}{1 - \dfrac{\gamma^2}{E - (\varepsilon_3 - \varepsilon_1)} G_{0(00)}(E)}, \tag{52}$$

where $G_{0(00)}(E)$ is defined by Eq. (17). Here, $G_{00}(E)$ has an extra pole at $E = (\varepsilon_3 - \varepsilon_1)$. The condition to get a localized state is

$$\frac{G_{0(00)}}{E - (\varepsilon_3 - \varepsilon_1)} = \frac{1}{\gamma^2}. \tag{53}$$

Let

$$E - (\varepsilon_3 - \varepsilon_1) = \pm \eta, \quad \eta \rightarrow 0,$$

and as $|G_{0(00)}(\varepsilon_3 - \varepsilon_1)|$ is bounded, then we get

$$E = \lim_{\eta \rightarrow 0}(\varepsilon_3 - \varepsilon_1) + \eta, \quad \frac{G_{0(00)}(\varepsilon_3 - \varepsilon_1)}{\eta} \uparrow \infty \tag{54}$$

and

$$E = \lim_{\eta \rightarrow 0}(\varepsilon_3 - \varepsilon_1) - \eta, \quad \frac{G_{0(00)}(\varepsilon_3 - \varepsilon_1)}{\eta} \downarrow -\infty. \tag{55}$$

So, even if $\gamma^2 \sim 0$, there will be a localized state at $(\varepsilon_3 - \varepsilon_1)$. In this limit, this is an atomic level state. This should be expected from the physical consideration also.

Case I.

$$(\varepsilon_3 - \varepsilon_1) > E_4 + \eta, \quad \eta \rightarrow 0.$$

Then, we shall have two more extra localized states below the bands. When $\gamma^2 \sim 0$, there will be a localized state in the band gap and it will appear below the lower band edge of the upper band (see Fig. 7, Case I). The atomic level localized state, as mentioned above, will be above the upper band edge. Figure 7(a) displays the plot of Eq. (53) for this case. Schematic representation of this case and cases II–V, discussed below, are shown in Fig. 7(b).

Case II.

$$(\varepsilon_3 - \varepsilon_1) < E_1 - \eta, \quad \eta \rightarrow 0.$$

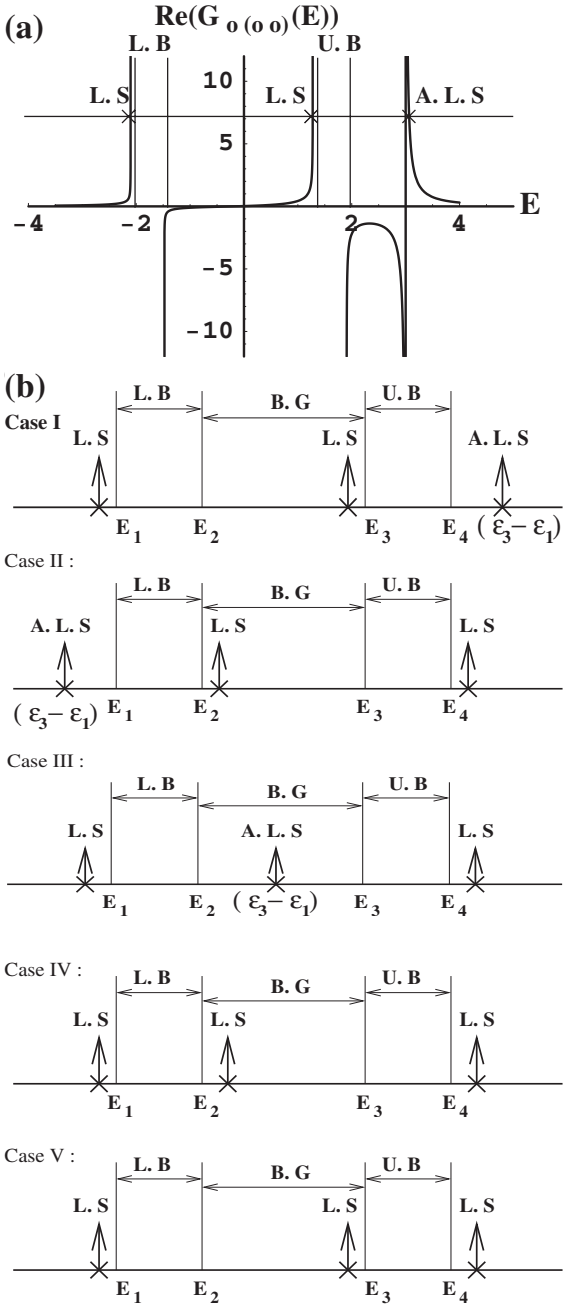

FIG. 7. (a) Plot of $\frac{G_{0(00)}(E)}{E-(\varepsilon_3-\varepsilon_1)}$ for the case when $(\varepsilon_3-\varepsilon_1)>E_4$, which shows where localized states (L. S) and atomic level state (A. L. S) can appear for this particular case. (b) shows the schematic representation of various cases [(I)–(V)] discussed in Sec. IV C. Here, we have marked the positions of the upper band (U. B), lower band (L. B), band gap (B. G), localized states (L. S) and atomic level states (A. L. S) on the energy axis coming for all the cases [(I)–(V)] in Sec. IV C, respectively.

In this case, we also have two more localized states above the bands with one in the band gap. When $\gamma^2 \sim 0$, one localized state will be just above the upper band edge of the lower band inside the gap. Note that in this case, we also have an atomic level localized state below the lower band (see Fig. 7, Case II).

Case III.

$$E_2 < (\varepsilon_3 - \varepsilon_1) < E_3.$$

As $\frac{1}{\gamma^2} > 0$, we have one localized state below the lower band edge of the lower band. One more localized state originates above the upper band edge of the upper band. Furthermore, we have one atomiclike localized state at $E=(\varepsilon_3-\varepsilon_1)$ (see Fig. 7, Case III). Note that this state is in the band gap.

Case IV.

$$E_1 < (\varepsilon_3 - \varepsilon_1) < E_2.$$

Note that the site energy of the dangling impurity is within the lower band. In this case, $G_{00}(E)$ is purely imaginary for $E_1 < E < E_2$. Again, $\frac{1}{\gamma^2} > 0$ will intersect $\frac{G_{00}(E)}{E-(\varepsilon_3-\varepsilon_1)}$ at $E=\lim_{\eta\to 0}[(\varepsilon_3-\varepsilon_1)+\eta]$ if the later is real. As in this case, $G_{00}(\varepsilon_3-\varepsilon_1)$ is not real, we can not have any atomiclike localized state from the interacting dangling impurity at $(\varepsilon_3-\varepsilon_1)$. As $\frac{1}{\gamma^2} > 0$, we shall have one localized state below the lower band edge of the lower band. One more localized state ensues above this band and in the band gap. However, a third localized state will appear above the upper band edge of the upper band. This can be seen from the real parts of $G_{0(00)}(E)$. So, there are still three localized states (see Fig. 7, Case IV).

Case V.

$$E_3 < (\varepsilon_3 - \varepsilon_1) < E_4.$$

Here, the site energy of the dangling impurity is within the upper band. Again in this case, we shall not have any atomiclike localized state at $E=(\varepsilon_3-\varepsilon_1)$. We will have one localized state below the lower band edge of the lower band. One more localized state appears below the lower band edge of the upper band. It is inside the band gap. Again, if $\gamma^2 \sim 0$, this localized state appears near the lower band edge. Furthermore, a third localized state appears above the upper band edge of the upper band (see Fig. 7, Case V).

The consideration of dangling bonds in the model gives rise to localized states, also within the band gap, just like the models represented by Figs. 2(c) and 2(d) and observed in the experiment. We note that the actual system is of two dimensions with approximately nanometer thick third dimension. So, there is a possibility of dangling bonds in the second dimension. In our case, the dangling bond density of Si(110)-(16×2) surface is larger than 0.5/atom^3. So, $\frac{1}{8}$ ML Ag could saturate only a fraction of them. This is primarily the motivation for considering a dangling bond impurity in the system.

E. Dangling bond at every (even) alternate lattice site

In this case, we consider that at every alternate lattice site, there is a dangling atom impurity which repeats throughout the whole lattice [see Fig. 2(f)]. Let us take the expression for the Green's function, as given in Eq. (17). Now, considering $\varepsilon_3=\varepsilon_2$ or $\varepsilon_3 \sim \varepsilon_2$ and $\gamma_{2n}=\gamma$, $\varepsilon_{3(2n)}=\varepsilon_3$, we get the expression for Green's function as

$$G_{00} = \pm \frac{E+2\varepsilon}{\sqrt{[(E+\varepsilon)^2-(4+\varepsilon^2+\gamma^2)][(E+\varepsilon)^2-(|\alpha-\beta|^2+\varepsilon^2+\gamma^2)]}}. \tag{56}$$

We write

$$E_1' = -\varepsilon - \sqrt{\varepsilon^2+\gamma^2+4}, \tag{57}$$

$$E_2' = -\varepsilon - \sqrt{\varepsilon^2+|\alpha-\beta|^2+\gamma^2}, \tag{58}$$

$$E_3' = -\varepsilon + \sqrt{\varepsilon^2+|\alpha-\beta|^2+\gamma^2}, \tag{59}$$

$$E_4' = -\varepsilon + \sqrt{\varepsilon^2+\gamma^2+4}, \tag{60}$$

which are the four real branch points of the Green's function.

So, for $E_2' < E < E_3'$, $E \in \mathbb{R}$, we write

$$G_{00}(E) = -\frac{E+2\varepsilon}{\sqrt{(E-E_1')(E-E_2')(E-E_3')(E-E_4')}}, \tag{61}$$

and for $E < E_1'$ and $E > E_4'$, $E \in \mathbb{R}$, we write

$$G_{00}(E) = \frac{E+2\varepsilon}{\sqrt{(E-E_1')(E-E_2')(E-E_3')(E-E_4')}}. \tag{62}$$

G_{00} for these energy ranges are real. Now, the density of states for the lower band ($E_1' < E < E_2'$, $E \in \mathbb{R}$) is

$$\rho_L(E) = \frac{1}{\pi}\frac{|E+2\varepsilon|}{\sqrt{(E-E_1')(E_2'-E)(E_3'-E)(E_4'-E)}}. \tag{63}$$

The density of states for the upper band ($E_3 < E < E_4$, $E \in \mathbb{R}$) is

$$\rho_u(E) = \frac{1}{\pi}\frac{|E+2\varepsilon|}{\sqrt{(E-E')(E-E_2')(E-E_3')(E_4'-E)}}. \tag{64}$$

The band gap is

$$\Delta = |E_3' - E_2'| = 2\sqrt{\varepsilon^2+|\alpha-\beta|^2+\gamma^2}. \tag{65}$$

So, the gap increases further due to the interaction from dangling atoms. The bandwidth is given by

$$(\mathrm{BW})_L = |E_2' - E_1'| = \sqrt{4+\varepsilon^2+\gamma^2} - \sqrt{|\alpha-\beta|^2+\varepsilon^2+\gamma^2} = (\mathrm{BW})_u. \tag{66}$$

If $|\gamma| \sim 0(1)$, we then write

$$\sqrt{4+\varepsilon^2+\gamma^2} - \sqrt{|\alpha-\beta|^2+\varepsilon^2+\gamma^2} \sim \sqrt{4+\varepsilon^2} - \sqrt{|\alpha-\beta|^2+\varepsilon^2} + \frac{1}{2}\gamma^2\left\{\frac{1}{\sqrt{4+\varepsilon^2}} - \frac{1}{\sqrt{|\alpha-\beta|^2+\varepsilon^2}}\right\}. \tag{67}$$

As $|\alpha-\beta|^2 < 4$, the second term in the parentheses is negative. So, the bandwidth decreases. We can conclude that further interaction with dangling atoms of second type reduces both bandwidths and increases the band gap.

Band gap (Δ) obtained from the model [Eq. (65)] described in this section is larger than that [Eq. (28)] obtained from the model in Fig. 2(b). It is known that dangling bonds are present on the Si(110)-(16×2) reconstructed surface,[3] and with a small coverage $\left(\frac{1}{8}\right)$ of Ag, all of them will not be saturated. Thus, different local environments exist on the surface, giving rise to variation of band gap. This model [Fig. 2(f)] also predicts a broadening of band gap as the model in Fig. 2(b) does. In the experiment, LDOS was obtained from various locations on the stripes of the (16×2) reconstructed surface, where local environment can be different. Thus, a band gap variation is expected.

F. Dangling bond periodicity at every (even) alternate lattice site: $\varepsilon_3 \neq \varepsilon_2$

So far, in all the calculations we did with dangling atom impurity, we have considered the case where $\varepsilon_3 = \varepsilon_2$ or $\varepsilon_3 \sim \varepsilon_2$. Now, let us see what happens when $\varepsilon_3 \neq \varepsilon_2$. This means that the site energy of dangling atom impurities, *C*, is different than the site energy of the atoms, *B*, which are sitting at the odd lattice sites. Now, with reference to Eq. (47), the calculation part, we proceed in the following way:

$$E - \Sigma(E) \pm 2\tilde{V}(E) = E - \frac{\alpha^2+\beta^2}{E+2E} - \frac{\gamma^2}{E-\varepsilon_3'} \pm 2\tilde{V}(E).$$

Here, we have used Eq. (13). After performing a trite algebra, we get

$$E - \Sigma(E) \pm 2\tilde{V}(E) = \frac{(\{(E+\varepsilon)^2 - [(\alpha \pm \beta)^2+\varepsilon^2+\gamma^2]\}(E-\varepsilon_3') - (\varepsilon_3'+2\varepsilon)\gamma^2)}{(E+2\varepsilon)(E-\varepsilon_3')} \tag{68}$$

[here, we have rewritten $\frac{E+2\varepsilon}{E-\varepsilon_3'}$ as $\frac{E+2\varepsilon}{E-\varepsilon_3'}+1-1=1+\frac{\varepsilon_3'+2\varepsilon}{E-\varepsilon_3'}$].

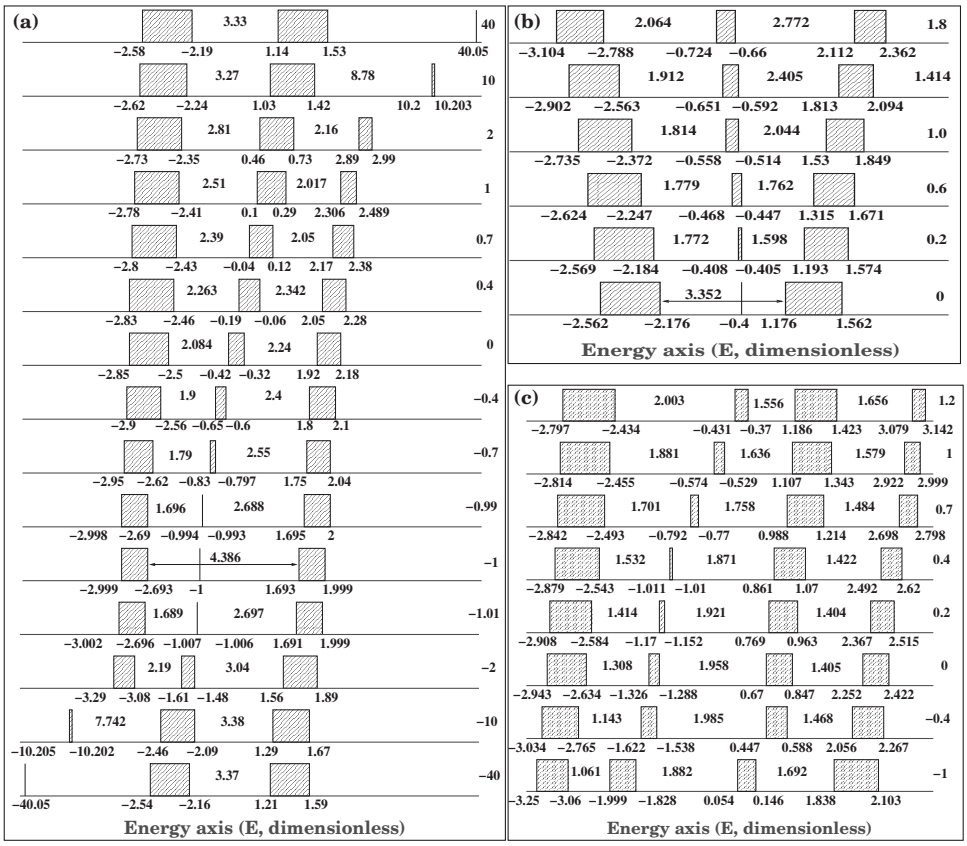

FIG. 8. Evolution of bands which are plotted by solving Eq. (69) for different values of (a) ε_3' and (b) γ and (c) by extending the dangling bond length vertically with four atoms per unit cell. For the band dynamics shown in (a), we have taken $(\alpha+\beta=2)$, $(\alpha-\beta=1.6)$ $\varepsilon=0.5$, and $\gamma=1.414$ and changed ε_3' as mentioned in the right side of the figure. (b) Evolution of bands plotted in a similar fashion as (a) by solving Eq. (69) for different values of γ. This particular set of solutions has been obtained by considering $(\alpha+\beta=2)$, $(\alpha-\beta=1.6)$, $\varepsilon=0.5$, and $\varepsilon_3'=-0.4$ and by changing the values of γ as mentioned in the right side of the figure. (c) This band dynamics was obtained by considering four atoms per unit cell. Otherwise, it is similar to (a). All the parameters here are the same as (a) with ε_3' changing as mentioned in the right side of the figure.

Let us consider a new variable

$$X = E - \varepsilon_3'.$$

Then, $E-\Sigma(E)\pm 2\tilde{V}(E)=0$ yields the following cubic equation in X:

$$X^3 + 2(\varepsilon_3' + \varepsilon)X^2 + [(\varepsilon_3' + \varepsilon)^2 - (\alpha \pm \beta)^2 - \varepsilon^2 - \gamma^2]X - (\varepsilon_3' + 2\varepsilon)\gamma^2 = 0. \quad (69)$$

This equation will have two cubic polynomials, one for $(\alpha+\beta)$ and the other for $(\alpha-\beta)$. Again, each of these polynomials will have three roots as this is a third order equation in X. This is further discussed in Appendix C. Therefore, for a particular value of ε_3', $(\alpha\pm\beta)$, ε, and γ, we get a total of six solutions in X. Now, for different values of ε_3', a series of solutions would be obtained for particular values of $(\alpha\pm\beta)$, ε, and γ. Since $X=E-\varepsilon_3' \Rightarrow E=X+\varepsilon_3'$, these six solutions represent six points in the energy (E) axis for each value of ε_3'. All of these quantities have been made dimensionless throughout of our whole calculation by V [see Eq. (8)]. These points would correspond to the maximum and minimum limits of the band edges in the energy axis and the band gaps associated with them. Figure 8(a) shows the schematic plot which is obtained for particular values of $(\alpha\pm\beta)$, ε, and γ but changing the ε_3' values. Here, ε_3' values were changed from −40 to +40, as shown in the right side of the figure. For $\varepsilon_3'=-1$, we get two bands at (−2.696, −2.999) and (1.693, 1.999) with a localized state at $E=-1$. This particular case is already discussed in Sec. II D. The width of both the bands for this particular value of ε_3' is the same and it is 0.306 (dimensionless). The band gap in this case is 4.386, which is the difference between the lower limit (−2,696) of the lower band and the lower limit (1.693) of the upper band. Now, when the value of ε_3' is increased from −1 to −0.99, we observe that the localized state which occurred at $E=-1$ for $\varepsilon_3'=-1$ now has a physical width of 0.0011 with a shift toward right (−0.9944, −0.9933) in the energy axis. The width of the right band (upper band) has reduced to 0.305 and it has also shifted toward the right of the energy axis and appears now at (1.695, 2). The width of the lower band increases to 0.308 from 0.306 and it is also shifted toward right, at (−2.998, −2.69). So, the main two bands show asymmetric bandwidths. At this point, one should note that in the STS spectra of the accompanying paper, indeed, asymmetric bandwidths are observed. In this way, when we keep

increasing the value of ε_3', we see that the localized state at $E=-1$ for $\varepsilon_3=-1$ now slowly gets the shape of a band with increasing value of ε_3', and the right band (upper band) width slowly decreases, whereas the left band (lower band) width slowly increases. The whole band structure gets shifted slowly toward right with increasing value of ε_3'. At a higher value of $\varepsilon_3'=10$, we can see that the right band (upper band) has shrunk to 0.003 (from 0.306), the middle band's (which was a localized state for $\varepsilon_3'=-1$ at $E=-1$) width has increased to 0.39, and that of the left band (lower band) to 0.38 from 0.306. In this way, the width of the right band (upper band) keeps decreasing asymptotically with higher values of ε_3' and when $\varepsilon_3'=40$, we get almost a localized state again at $E=40.05$. Width of the left band (lower band) and the middle band now becomes equal, which is 0.39, and the band gap between these two bands decreases now to 3.33 from 4.386 when $\varepsilon_3'=40$. The variation of the width of the bands is associated with the states coming out from one band and joining the other, resulting in the increase or decrease of a bandwidth.

Similarly, when the value of ε_3' decreases further from -1, we see that the localized state at $E=-1$ for $\varepsilon_3'=-1$ again slowly increases its width but this time at the expense of the left band (lower band). In fact, the width of the left band (lower band) slowly decreases, whereas those of the middle band and the right band (upper band) slowly increase with decreasing value of ε_3'. The whole band structure in this case slowly shifts toward the left of the energy axis with decreasing ε_3'. In this way, when $\varepsilon_3'=-40.00$, we get a localized state at $E=-40.05$ and the width of the middle band and the upper band again becomes equal and it is 0.38 with a band gap of 3.37 in between them. Therefore, it shows the evolution of the bands with ε_3' keeping the parameters $(\alpha \pm \beta)$, ε, and γ fixed at their particular values.

In the second case, we have kept the value of ε_3' fixed at -0.4 but changed the parameter γ, which is the interaction parameter between the dangling atom, C, and the even site atom, A. The values of $(\alpha \pm \beta)$ and ε are kept the same as in the previous case. Figure 8(b) shows the schematic plot of the band dynamics where γ has been changed from 1.8 to 0.0. For $\gamma=0$, we get a localized state at $E=-0.4$ and the width of the lower and upper bands is equal for this particular value of γ and it is 0.386. As the γ value increases from 0.0 to 1.8, both the bands (lower and upper) start shrinking, whereas the localized state is slowly taking the band's shape.

Now, to correlate the results from the theoretical model and the experimental results coming from STS measurements, two prominant bands are associated with one or more than one small states in between them in the experimental STS spectra. We address these two prominent bands as the highest occupied subband (HOS) and lowest unoccupied subband (LUS). In the STS spectra, the widths of the HOS and LUS vary. Also, the widths of the states arising between HOS and LUS vary. Therefore, it is more likely that the STS spectra have been acquired in the regime where mostly the ε_3' and γ have the values for which we get two prominent bands with states or a small band in between. So, this could be a direct correspondence of the electronic properties of Ag deposited on nanowirelike Si(110)-(16×2) structures with the theoretical model calculations.

G. Vertical extension of the dangling bond periodicity at every even lattice site

Here, we consider a model in which a chain of two identical dangling atoms is attached to every even lattice sites, A, as shown in Fig. 2(h). We assume here that the length of both the bonds in the dangling is the same. Therefore, in this model, the total dangling bond length is extended vertically and it is now double the length of the previous cases. However, all other parameters are considered similar as before with $\varepsilon_3 \neq \varepsilon_2$. So, the number of atoms per unit cell, in this case, becomes 4 instead of 3 as considered before. The amplitude equations of electrons are given by

$$i\frac{dC_{2n}}{d\tau} = \beta C_{2n+1} + \alpha C_{2n-1} + \gamma_{2n} X_{2n}, \tag{70}$$

$$i\frac{dC_{2n+1}}{d\tau} = -2\varepsilon C_{2n+1} + \alpha C_{2n+2} + \beta C_{2n},$$

$$n = 0, \pm 1, \pm 2, \ldots, \tag{71}$$

$$i\frac{dX_{2n}}{d\tau} = \gamma_{2n} C_{2n} + (\varepsilon_3 - \varepsilon_1) X_{2n} + \gamma_{2n} Y_{2n}, \tag{72}$$

$$i\frac{dY_{2n}}{d\tau} = \gamma_{2n} X_{2n} + (\varepsilon_3 - \varepsilon_1) X_{2n}. \tag{73}$$

Note that two dangling sites are denoted by X and Y, respectively. Now, proceeding in a similar fashion as before by performing first Laplace tranformation and then renormalizing the lattice, we get the expression for $\Sigma_n(E)$ as

$$\Sigma_n(E) = \frac{\alpha^2 + \beta^2}{E + 2\varepsilon} + \frac{\gamma_n^2}{E - \varepsilon_3' - \dfrac{\gamma_n^2}{E - \varepsilon_3'}}. \tag{74}$$

So, putting this expression of $\Sigma_n(E)$ in Eq. (18) and solving it with $\gamma_n = \gamma$, we get a total of eight solutions for energy. This corresponds to four energy bands and three band gaps associated with the bands for a particular value of ε, γ_n, α, β, and ε_3'. These results are consistent with the model of four atoms per unit cell. Solving Eq. (11) for different values of ε_3', we can see how the bands evolve with ε_3'. Schematic plot of the bands are shown in Fig. 8(c).

In Fig. 8(c), one can see that when the value of ε_3' decreases from 0.4, the width of the first band (lowest band) decreases, whereas the width of the second band (next upper band) increases. This implies that the states from the tail of the first band are coming out and they are getting attached to the second band. As a result, the width of the second band increases. On the other hand, in between the third (next to the next upper band) and fourth (uppermost, highest band) bands, the width of the third band decreases, whereas the width of the fourth band increases, which implies that the states from the tail of the third band are coming out and going to the fourth band when the value of ε_3' decreases from 0.4 to -1. The other way of thinking about it is as follows. States from the second band are coming out and going to the

first band and the states from the fourth band are coming out and attaching to the third band as the value of ε_3' increases from -1 to 0.4. At $\varepsilon_3'=0.4$, the second band is almost like a localized state with a width of 0.001. It is an atomiclike state. For a single atom dangling chain, we have analytically showed it in Sec. II E. It happens there as $\varepsilon_3'=-1$ and $\varepsilon_3=\varepsilon_2$. In this limit, we have three bands there. When the value of ε_3' increases further from 0.4, one can see that the band splitting now solely occurs from the fourth band. The width of the fourth band (uppermost band) decreases, whereas the widths of all other three bands increase gradually with the increase of ε_3'. Another interesting thing which should be noted here is that the value of the total band gap increases with increasing ε_3'. At $\varepsilon_3'=1.2$, the total band gap (sum total of all the three gaps) is 5.215, whereas it is 4.635 at $\varepsilon_3'=-1$. For $\varepsilon_3'=0.4$, the total band gap is 4.825. Therefore, in this model with four atoms per unit cell, the over all band gap has increased further for the same range of parameter values. We close this section by noting the following. The STS spectra of Ag-adsorbed Si surface show more than two bands. Of course, two bands are most prominent in the spectra. This analysis shows that the presence of these extra bands or bandlike structures must be due to long dangling chains in the system. A model with a distribution of dangling bond lengths will be useful to further understand the experimental findings discussed here.

H. Many dangling atom interaction at every even site

Here, we consider a situation where at every even site M number of identical dangling atoms interact with the lattice site [see Fig. 2(i)]. For this model, the equations of motion are given by the following set:

$$i\frac{dC_{2n}}{d\tau}=\beta C_{2n+1}+\alpha C_{2n-1}+\gamma\sum_{m=1}^{M}X_{2n,m}, \tag{75}$$

$$i\frac{dC_{2n+1}}{d\tau}=-2\varepsilon C_{2n+1}+\alpha C_{2n+2},$$

$$i\frac{dX_{2n,m}}{d\tau}=\gamma C_{2n}+\varepsilon_3 X_{2n,m}. \tag{76}$$

We now have

$$i\frac{d}{d\tau}\sum_{m=1}^{M}X_{2n,m}=\gamma M C_{2n}+\varepsilon_3\sum_{m=1}^{M}X_{2n,m}.$$

So, the analysis will remain the same, except that γ will be replaced by γM. Consequently, even if $\gamma\sim O(1)$, but M is large such that $\gamma M\sim O(1)$, there will be an appreciable increase of the band gap when $\varepsilon_3=\varepsilon_2$ or $|M^2\gamma^2(\varepsilon_3-\varepsilon_1)|\sim O(1)$. However, in the case of $\varepsilon_3\neq\varepsilon_2$, there will be three bands and two band gaps. These two band gaps will vanish with the appearance of a single band gap when $\varepsilon_3\sim\varepsilon_2$ or $|\gamma(\varepsilon_3-\varepsilon_2)|\sim O(1)$.

III. SUMMARY AND CONCLUSIONS

We have presented a one-dimensional tight-binding model using the Green function formalism. Various cases of this model have been investigated. The results from this model provide a qualitative understanding of the experimental results obtained on a Si(110)-(16×2) reconstructed surface. Electronic structures of the Si(110)-(16×2) reconstructed surface and a low-coverage Ag-adsorbed Si(110)-(16×2) reconstructed surface were investigated by scanning tunneling spectroscopy. Electronic local density of states has been probed by the measurement of conductance. Local density of states on the nanowire-like stripes of Si on the (16×2) reconstructed bare Si(110) surface shows a band gap comparable to that for bulk Si. Upon low-coverage ($\frac{1}{8}$ ML) Ag adsorption at room temperature on this surface, LDOS, in general, shows a wider band gap compared to the bare surface. A variation of band gap has been observed when LDOS has been obtained from different spatial locations. If the Fermi level of the system is defined at the middle of the band gap, then a variation of the position of the Fermi level has been observed. In addition, new electronic states appear within the band gap. Many features of similar problems can be investigated by this model. For example, the effect of various types of sequences in the dangling or side chains can be investigated. Though not investigated here, the effect of length disorder of the side chain on the spectra can also be investigated. All these features are qualitatively understood from the model we presented here. Experimentally, a low-coverage ($\frac{1}{8}$ ML) Ag deposition was used to capture a wide variation of local electronic structure as STS probes LDOS. Such a small coverage is much smaller than the dangling bond density[3] [0.625/atom]. Many variants of our 1D model is capable of capturing the essence of the experiment.

Density functional method can provide more quantitative results. However, at present, there is no well-accepted structural model even for the clean Si(110)-(16×2) reconstructed surface. Treating the case of Ag adsorption on this surface introduces additional complexity for this system to be treated by density functional theory (DFT) method at this state. However, we plan to investigate this problem by DFT method in the near future. Again, we emphasize that the present model, though parametric, can explain the experimental results qualitatively and will be a good theoretical guide for experimentalists in this field.

APPENDIX A: DERIVATION OF AMPLITUDE EQUATIONS FROM THE TIGHT-BINDING HAMILTONIAN

We consider a bipartite one-dimensional chain. This system is considered to have dangling or side chains of various sizes from every alternate sites. The tight-binding Hamiltonian for this system is proposed. Amplitude equations are then derived.

To describe the quantum dynamics of a particle in the system under consideration, we propose the following tight-binding Hamiltonian H. In this Hamiltonian, only nearest-neighbor tunneling of the particle is allowed,

$$H = \sum_{i=0}^{3} H_i, \tag{A1}$$

$$H_0 = \sum_n \mathcal{E}_{(n,0)} |n,0\rangle\langle n,0|, \quad n \in Z, \tag{A2}$$

$$H_1 = \sum_n \sum_{m=1}^{N_{2n}} \mathcal{E}_{3(2n,m)} |2n,m\rangle\langle 2n,m|, \quad n \in Z, \quad N_{2n} \in Z_+, \tag{A3}$$

$$H_2 = \sum_n \sum_m V_{(n,0)(m,0)} [\delta_{n,m+1} + \delta_{n,m-1}] |n,0\rangle\langle m,0|, \quad n,m \in Z, \tag{A4}$$

$$H_3 = \sum_n \sum_{i,j=0}^{N_{2n}} V_{3(2n,i)(2n,j)} [\delta_{i,j+1} + \delta_{i,j-1}] |2n,i\rangle\langle 2n,j|, \tag{A5}$$

$$n \in Z, \quad N_{2n} \in Z_+.$$

Here, $|n,m\rangle$ denotes a one particle Wannier ket[11] state, which is localized at the (n,m) site of the lattice. We note that $(n,0)$ denotes the coordinate of the lattice along the horizontal or the primary chain. This is taken to be a bipartite lattice, i.e., *ABABAB*…. We give coordinates $(2n,0)$ to the A sites, as a choice with a B site having the coordinate $(2n+1,0)$. So, $(2n,m)$ denotes the mth site of the dangling or side chain, which originates from the $(2n,0)$th site or from an A site of the primary chain. In this Hamiltonian, $N_{2n} \in Z_+$ denotes the number of lattice sites on the dangling chain, originated from the $(2n,0)$th site of the system. This quantity can, in principle, be a random variable. Other parameters in the Hamiltonian have their usual meaning, as in any tight-binding Hamiltonian. We note in this context that Wannier states belonging to different lattice sites are orthogonal.[11] These states, in fact, form a complete orthonormal set. So, $\langle n,m|l,k\rangle = \delta_{n,l}\delta_{m,k}$.

Now, let $|\Psi\rangle(t) = |\Phi_1\rangle(t) + |\Phi_2\rangle(t)$ denote an arbitrary state of the one particle system at a time t, where we define $|\Psi\rangle(t)$ as follows.

$$|\Phi_1\rangle(t) = \sum_{n_1} C_{(n_1,0)}(t) |n_1,0\rangle, \tag{A6}$$

$$|\Phi_2\rangle(t) = \sum_{n_1} \sum_{m_1=1}^{N_{2n_1}} X_{(2n_1,m_1)}(t) |2n_1,m_1\rangle. \tag{A7}$$

From these, we further have the following equations:

$$\langle l,0|\Phi_1\rangle(t) = \sum_{n_1} C_{(n_1,0)}(t)\langle l,0|n_1,0\rangle = C_{(l,0)}, \tag{A8}$$

$$\langle l,0|\Phi_2\rangle(t) = 0, \tag{A9}$$

$$\langle 2l,m|\Phi_1\rangle(t) = 0 = \langle 2l+1,m|\Phi_1\rangle(t), \tag{A10}$$

$$\langle 2l,m|\Phi_2\rangle(t) = \sum_{n_1} \sum_{m_1=1}^{N_{2n_1}} X_{(2n_1,m_1)}(t)\langle 2l,m|2n_1,m_1\rangle = X_{(2l,m)}(1-\delta_{m,0}), \tag{A11}$$

$$\langle 2l+1,m|\Phi_2\rangle(t) = \sum_{n_1} \sum_{m_1=1}^{N_{2n_1}} X_{(2n_1,m_1)}(t)\langle 2l+1,m|2n_1,m_1\rangle = 0. \tag{A12}$$

Here, $C_{(l,0)}(t)$ is the amplitude of the particle at the lth site of the primary chain. Similarly, $X_{(2n,m)}$ is the amplitude of the particle at the mth site of the dangling chain, emanated from the $(2n,0)$th site of the primary chain.

We now consider

$$H|\Psi\rangle = \sum_{i=0}^{3} H_i(|\Phi_1\rangle + |\Phi_2\rangle). \tag{A13}$$

After some trite algebra, we get the following results:

$$H_0|\Phi_1\rangle = \sum_{n,n_1} \mathcal{E}_{(n,0)} C_{(n_1,0)}(t) |n,0\rangle\langle n,0|n_1,0\rangle = \sum_n \mathcal{E}_{n,0} C_{(n,0)}(t) |n,0\rangle, \tag{A14}$$

$$H_0|\Phi_2\rangle = \sum_{n,n_1} \sum_{m_1=1}^{N_{2n_1}} \mathcal{E}_{n,0} X_{(2n_1,m_1)}(t)\langle n,0|2n_1,m_1\rangle |n,0\rangle = 0, \tag{A15}$$

$$H_1|\Phi_1\rangle = \sum_n \sum_{m=1}^{N_{2n}} \sum_{n_1} \mathcal{E}_{3(2n,m)} C_{(n_1,0)}(t)\langle 2n,m|n_1,0\rangle |2n,m\rangle = 0. \tag{A16}$$

The origin of nullity in the first case is the absence of $m_1 = 0$ term in the third sum. The other equation gives zero due to the absence of $m=0$ term in the sum in H_1,

$$H_1|\Phi_2\rangle = \sum_{n,n_1} \sum_{(m,m_1)=(1,1)}^{(N_{2n},N_{2n_1})} \mathcal{E}_{3(2n,m)} X_{(2n_1,m_1)}(t) \times \langle 2n,m|2n_1,m_1\rangle |2n,m\rangle = \sum_n \sum_{m=1}^{N_{2n}} \mathcal{E}_{3(2n,m)} X_{(2n,m)}(t) \times |2n,m\rangle, \tag{A17}$$

$$H_2|\Phi_1\rangle = \sum_{n,n_1,m} V_{(n,0)(m,0)} C_{(n_1,0)}(t)[\delta_{n,m+1} + \delta_{n,m-1}] \times \langle m,0|n_1,0\rangle |n,0\rangle = \sum_n [V_{(n,0)(n-1,0)} C_{(n-1,0)}(t) + V_{(n,0)(n+1,0)} C_{(n+1,0)}(t)] |n,0\rangle, \tag{A18}$$

$$H_2|\Phi_2\rangle = \sum_{n,m,n_1} \sum_{m_1=1}^{N_{2n_1}} \{V_{(n,0)(m,0)} X_{(2n_1,m_1)}(t)[\delta_{n,m+1} + \delta_{n,m-1}] \times \langle m,0|2n_1,m_1\rangle |n,0\rangle\} = 0. \quad \text{(A19)}$$

We note that the last equation yields zero due to the absence of $m_1=0$ in the last sum,

$$H_3|\Phi_1\rangle = \sum_{n,n_1} \sum_{i,j=0}^{N_{2n}} V_{3(2n,i)(2n,j)} C_{(n_1,0)}(t)[\delta_{i,j+1} + \delta_{i,j-1}] \times |2n,i\rangle\langle 2n,j|n_1,0\rangle = \sum_{n} \sum_{i=0}^{N_{2n}} V_{3(2n,i)(2n,0)} C_{(2n,0)}(t) \times [\delta_{i,1} + \delta_{i,-1}]|2n,i\rangle = \sum_{n} V_{3(2n,1)(2n,0)} C_{(2n,0)}(t) \times |2n,1\rangle, \quad \text{(A20)}$$

$$H_3|\Phi_2\rangle = \sum_{n,n_1} \sum_{i,j=0}^{N_{2n}} \sum_{m_1=1}^{N_{2n_1}} \{V_{3(2n,i)(2n,j)} X_{(2n_1,m_1)}(t)[\delta_{i,j+1} + \delta_{i,j-1}] \times |2n,i\rangle\langle 2n,j|2n_1,m_1\rangle\} = \sum_{n} \sum_{i=0}^{N_{2n}} \sum_{j=1}^{N_{2n}} V_{3(2n,i)(2n,j)} X_{(2n,j)}(t)[\delta_{i,j+1} + \delta_{i,j-1}]|2n,i\rangle = \sum_{n} \left[\sum_{i=2}^{N_{2n}} V_{3(2n,i)(2n,i-1)} X_{(2n,i-1)}(t) + \sum_{i=0}^{N_{2n}} V_{3(2n,i)(2n,i+1)} X_{(2n,i+1)}(t) \right] |2n,i\rangle. \quad \text{(A21)}$$

We now derive the following important equations:

$$\langle l,0|H_0|\Phi_1\rangle = \mathcal{E}_{(l,0)} C_{(l,0)}(t), \quad \text{(A22)}$$

$$\langle l,0|H_0|\Phi_2\rangle = 0, \quad \text{(A23)}$$

$$\langle l,0|H_1|\Phi_1\rangle = 0, \quad \text{(A24)}$$

$$\langle 2l,m|H_1|\Phi_2\rangle = \mathcal{E}_{3(2l,m)} X_{(2l,m)}\ (t))(1-\delta_{m,0}), \quad \text{(A25)}$$

$$\langle 2l+1,m|H_1|\Phi_2\rangle = 0, \quad \text{(A26)}$$

$$\langle l,0|H_2|\Phi_1\rangle = V_{(l,0)(l-1,0)} C_{(l-1,0)}(t) + V_{(l,0)(l+1,0)} C_{(l+1,0)}(t), \quad \text{(A27)}$$

$$\langle l,0|H_2|\Phi_2\rangle = 0, \quad \text{(A28)}$$

$$\langle 2l,m|H_3|\Phi_1\rangle = V_{3(2l,1)(2l,0)} C_{(2l,0)}(t)\delta_{m,1}, \quad \text{(A29)}$$

$$\langle 2l+1,m|H_3|\Phi_1\rangle = 0, \quad \text{(A30)}$$

$$\langle 2l,m|H_3|\Phi_2\rangle = V_{3(2l,m)(2l,m-1)} X_{(2l,m-1)}(t)(1-\delta_{m,0}-\delta_{m,1}) + V_{3(2l,m)(2l,m+1)} X_{(2l,m+1)}(t), \quad \text{(A31)}$$

$$\langle 2l+1,m|H_3|\Phi_2\rangle = 0. \quad \text{(A32)}$$

To obtain the desired amplitude equations, we use the time dependent Schrödinger equation

$$\imath\hbar \frac{\partial|\Psi\rangle}{\partial t} = H|\Psi\rangle = \sum_{i=0}^{3} H_i(|\Phi_1\rangle + |\Phi_2\rangle). \quad \text{(A33)}$$

Required matrix elements are calculated to obtain the time dependent equations for $C_{(2l,0)}$, $C_{(2l+1,0)}$, and $X_{(2l,m)}$, $1 \leqslant m \leqslant N_{2l}$, $l \in Z$. These equations are given as follows:

$$\imath\hbar \frac{\partial C_{(2l+1,0)}}{\partial t} = \mathcal{E}_{(2l+1,0)} C_{(2l+1,0)} + V_{(2l+1,0)(2l,0)} C_{(2l,0)} + V_{(2l+1,0)(2l+2,0)} C_{(2l+2,0)}, \quad \text{(A34)}$$

$$\imath\hbar \frac{\partial C_{(2l,0)}}{\partial t} = \mathcal{E}_{(2l,0)} C_{(2l,0)} + V_{(2l,0)(2l-1,0)} C_{(2l-1,0)} + V_{(2l,0)(2l+1,0)} C_{(2l+1,0)} + V_{3(2l,0)(2l,1)} X_{(2l,1)}, \quad \text{(A35)}$$

$$\imath\hbar \frac{\partial X_{(2l,m)}}{\partial t} = \mathcal{E}_{3(2l,m)} X_{(2l,m)}(1-\delta_{m,0}) + V_{3(2l,m)(2l,m-1)} X_{(2l,m-1)}(1 - \delta_{m,0} - \delta_{m,1}) + V_{3(2l,m)(2l,m+1)} X_{(2l,m+1)} \times (1-\delta_{m,0}) + V_{3(2l,1)(2l,0)} C_{(2l,0)} \delta_{m,1}(1-\delta_{m,0}). \quad \text{(A36)}$$

In the models discussed in the text, $N_{2n}=N$, $\forall n$. Furthermore, only cases for $N=1$ and 2 are considered. $V_{3(2l,m)}=V_3$, $\forall m \geqslant 1$. $V_{(2n,2n+1)}=V_1$ and $V_{(2n-1,2n)}=V_2$, $\forall n \in Z$. $\mathcal{E}_{(2n,0)}=\mathcal{E}_1$, $\forall n \in Z$. $\mathcal{E}_{(2n+1,0)}=\mathcal{E}_1$ or $\mathcal{E}_2$, $\forall n \in Z$, depending on whether the sample is pristine or not. $\mathcal{E}_{3(2n,m)}=\mathcal{E}_3$, $\forall n \in Z$, and $m \in N$.

APPENDIX B

From Eqs. (30)–(33) in the text, we have the equations Eqs. (34)–(36) for Green's function after performing the Laplace transformation with respect to E and then renormalizing the lattice as mentioned before. The schematic representation of this case is shown in Fig. 6. The operator expression for the Green's function G is

$$G(E) = (E-H)^{-1}. \quad \text{(B1)}$$

Here, H is the Hamiltonian operator which is given by $H=H_0+H_1$ and $G_0(E)=(E-H_0)^{-1}$. Therefore, we can write Eq. (B1) as

$$G(E) = (E-H_0-H_1)^{-1}. \quad \text{(B2)}$$

After performing a simple algebra on Eq. (B2), we get the standard Dyson equation,[12] which reads

$$G = G_0 + G_0 H_1 G. \quad \text{(B3)}$$

In the site representation (using Wannier kets, say),

$$G_{nm} = G_{0nm} + \Sigma_{l,k} G_{0nl} H_{lk} G_{km}, \quad \text{(B4)}$$

where we define H as

$$[H_0(E)]_{nm} = \Sigma(E)\delta_{nm} + \tilde{V}(E)(\delta_{n+1,m} + \delta_{n-1,m}), \quad \text{(B5)}$$

$$[H_1(E)]_{nm} = [\delta\Sigma_0(E)\delta_{n,0} + \delta\Sigma_1(E)\delta_{n,1}]\delta_{n,m} + \delta\tilde{V}_{nm}(E) \times (\delta_{n+1,m}\delta_{n,0} + \delta_{n-1,m}\delta_{n,1}). \quad \text{(B6)}$$

So, the components of H are given by

$$[H_1(E)]_{00} = \delta\Sigma_0(E), \quad \text{(B7)}$$

$$[H_1(E)]_{11} = \delta\Sigma_1(E), \quad \text{(B8)}$$

$$[H_1(E)]_{01} = \delta\tilde{V}_{0,1}(E), \quad \text{(B9)}$$

$$[H_1(E)]_{10} = \delta\tilde{V}_{1,0}(E). \quad \text{(B10)}$$

Note that the matrix representations are derived using Wannier kets.[11]

APPENDIX C

Equation (70) in the text reads as

$$X^3 + 2(\varepsilon_3' + \varepsilon)X^2 + [(\varepsilon_3' + \varepsilon)^2 - (\alpha \pm \beta)^2 - \varepsilon^2 - \gamma^2]X - (\varepsilon_3' + 2\varepsilon)\gamma^2 = 0. \quad \text{(C1)}$$

Now, let us define

$$a_0 = -(\varepsilon_3' + 2\varepsilon)\gamma^2,$$

$$a_1 = (\varepsilon_3' + \varepsilon)^2 - (\alpha \mp \beta)^2 - \varepsilon^2 - \gamma^2,$$

$$a_2 = 2(\varepsilon_3' + \varepsilon),$$

$$q = \frac{1}{3}a_1 - \frac{1}{9}a_2^2 = \frac{1}{3}\left[(\alpha \mp \beta)^2 + \varepsilon^2 + \gamma^2 + \frac{1}{3}(\varepsilon_3' + \varepsilon)^2\right],$$

$$r = \frac{1}{6}(a_1a_2 - 3a_0) - \frac{1}{27}a_2^3 = \frac{1}{27}(\varepsilon_3' + \varepsilon)^3 - \frac{1}{3}(\varepsilon_3' + \varepsilon)[(\alpha \mp \beta)^2 + \varepsilon^2 + \gamma^2] + \frac{1}{2}(\varepsilon_3' + 2\varepsilon)\gamma^2.$$

After a trite algebra, we get

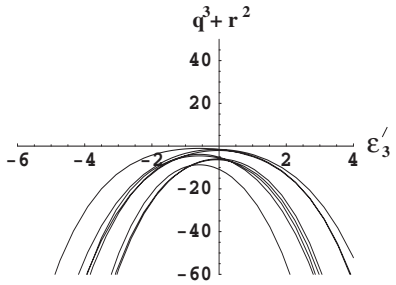

FIG. 9. Plot of the polynomial given by Eq. (55) in Appendix C. q^3+r^2 is plotted with respect to ε_3' for different values of the parameters $(\alpha \pm \beta)$, ε, and γ. It shows that for any value of the parameters, the roots of the polynomial are always real.

$$q^3 + r^2 = -\frac{1}{27}[(\alpha \pm \beta)^2 + \varepsilon^2 + \gamma^2][(\alpha \pm \beta)^2 + \varepsilon^2 + \gamma^2 + (\varepsilon_3' + \varepsilon)^2]^2 - \frac{1}{12}[\varepsilon_3'^2 - (2\varepsilon)^2]\gamma^4 + \frac{1}{27}(\varepsilon_3' + \varepsilon) \times (\varepsilon_3'^2 - 4\varepsilon^2)(\varepsilon_3' + 4\varepsilon)\gamma^2 - \frac{1}{3}(\varepsilon_3' + \varepsilon)(\varepsilon_3' + 2\varepsilon) \times (\alpha \pm \beta)^2\gamma^2. \quad \text{(C2)}$$

Case I.

We note that if $(\varepsilon_3'+2\varepsilon)=0 \Rightarrow \varepsilon_3=\varepsilon_1$, then $q^3+r^2<0$.[13] So, all three roots are real. This is already established through exact calculation. The same is true if $\gamma=0$.

Case II. Now, when $\varepsilon_3'=2\varepsilon \Rightarrow \varepsilon_3-\varepsilon_1=\varepsilon_1-\varepsilon_2 \Rightarrow \varepsilon_1=\frac{\varepsilon_2+\varepsilon_3}{2}$, again we get

$$q^3 + r^2 = -\frac{1}{27}[(\alpha \pm \beta)^2 + \varepsilon^2 + \gamma^2][(\alpha \pm \beta)^2 + 10\varepsilon^2 + \gamma^2]^2 - 4\varepsilon^2(\alpha \pm \beta)^2\gamma^2 < 0. \quad \text{(C3)}$$

So, when $\varepsilon_1=\frac{\varepsilon_2+\varepsilon_3}{2}$, all roots are again real. Now, let us see what happens in the most general case. To check that, we have plotted the polynomial (q^3+r^2) with respect to ε_3' as given by Eq. (I.162) for different values of the parameters $(\alpha \pm \beta)$, ε, and γ. The plot is shown in Fig. 9. From the plot, we see that we always get $q^3+r^2<0$ for a range of the values of the parameters considered here. It indicates that $q^3+r^2<0$ is most likely valid in the most general case. This will also be consistent with the requirement of models considered here.

*bhupen@iopb.res.in; msbnd@iacs.res.in

[1] *Green's Functions in Quantum Physics*, 2nd ed., edited by E. N. Economou (Springer-Verlag, Berlin, 1983).
[2] Samar Chattopadhyay, Ph.D. thesis, University of Kalyani, 2005.
[3] W. E. Packard and J. D. Dow, Phys. Rev. B **55**, 15643 (1997).
[4] E. J. van Loenen, D. Dijkkamp, and A. J. Hoeven, J. Microsc. **152**, 487 (1988).
[5] T. An, M. Yoshimura, I. Ono, and K. Ueda, Phys. Rev. B **61**, 3006 (2000).
[6] A. A. Stekolnikov, J. Furthmuller, and F. Bechstedt, Phys. Rev. Lett. **93**, 136104 (2004).
[7] P. K. Datta, D. Giri, and K. Kundu, Phys. Rev. B **47**, 10727 (1993); K. Kundu, D. Giri, and K. Ray, J. Phys. A **29**, 5699 (1996).
[8] D. H. Dunlap, H. L. Wu, and P. W. Phillips, Phys. Rev. Lett. **65**, 88 (1990).

[9] Arunava Chakrabarti and S. N. Karmakar, Phys. Rev. B **44**, 896 (1991).
[10] Gordon Baym, *Lectures on Quantum Mechanics* (Benjamin/Cummings, Menlo Park, CA, 1973), p. 118.
[11] C. Kittle, *Quantum Theory of Solids* (Wiley, New York, 1963), p. 195.
[12] J. M. Ziman, *Elements of Advanced Quantum Theory* (Cambridge University Press, Cambridge, 1969), p. 91.
[13] M. Abramowitz and Irene A. Stegun, *Handbook of Mathematical Functions* (Dover, New York, 1970), p. 17.